Nitrogen Oxyanion Reductive Borylation at Low-Coordinate Iron: A Struggle Between Two Oxophiles

Bao G. Tran,† Nobuyuki Yamamoto,† Maren Pink,† Yaroslav Losovyj,†,‡ Kenneth G. Caulton†,* and Jeremy M. Smith†,*

† Department of Chemistry, Indiana University, 800 E. Kirkwood Avenue, Bloomington, Indiana 47405, United States

‡ Department of Physics and Astronomy, University of Nebraska, Lincoln 68588, Nebraska, United States

Corresponding Authors: Kenneth G. Caulton. caulton@iu.edu, Jeremy M. Smith. smith962@iu.edu

ABSTRACT: With the advent of the Haber-Bosch process over a century ago, the world's population experienced tremendous growth due to the million tons of fixed nitrogen used in fertilizer each year. However, the majority of the fixed nitrogen is metabolized to various nitrogen oxyanions by soil organisms and find themselves lost in waterways, leading to eutrophication and hypoxia. Therefore, there is a need to convert the anthropogenic nitrogen content to more useful forms. In this work, the synthesis and characterization of an iron nitrate ($PhB(^{i}Pr_2Im)_3FeNO_3$) complex (**2**) is reported. Subsequent stepwise deoxygenation via a bis(boryl) reduced N-heterocycle ($BPin_2pz$) to their downstream counterparts was shown to be thermodynamically favorable by DFT. Reaction of iron nitrate with ($BPin_2$)pz led to the formation of an iron (pinacolato)boralanolate complex (**3**) and a diiron dinitrosyl with bridged hydroxide ligands ($[PhB(^{i}Pr_2Im)_3Fe(NO)(OH)]_2$) (**4**). The formation of these complexes demonstrates the oxophilicity of both iron and boron. Overall, this remarkable reactivity of iron nitrate showed that this is a viable method for converting the environmentally harmful nitrate anion into a more interesting form of nitrogen.

INTRODUCTION

Over the last few decades, anthropogenic activities have dramatically increased the concentration of reactive nitrogen in the environment, notably in the form of nitrate and nitrite. This meteoric rise is in part a consequence of industrial agriculture[1] that uses industrially produced Haber-Bosch ammonia to deliver nitrogen-based fertilizers. While this ammonia fertilizer is critical for maintaining the world's population, most of this applied nitrogen fertilizer is not absorbed by crops. In fact, over 80 % is lost to the environment through runoff, leaching, volatilization, and denitrification processes.[2,3] This microbial oxidation of ammonia produces a surfeit of nitrogen oxyanions that accumulate in the environment and overwhelm natural denitrification processes, ultimately leading to the eutrophication of waterways,[4] which is most noticeable in coastal waters.[5] These aquatic dead zones have deleterious effects on aquatic species through habitat loss or the compression and reduction of biomass. For example, hypoxia hinders the spawning of cod in the Baltic Sea at the depths where the water salinity provides buoyancy for their eggs.[6]

Artificial denitrification processes represent one strategy to combat a plethora of looming environmental problems. For example, both heterogeneous and molecular electrocatalysts have been demonstrated to reduce aqueous nitrate to species with lower nitrogen oxidation states, including ammonia and hydroxylamine. Despite extensive mechanistic investigations, insight into the factors that control product selectivity in electrocatalysis is often limited by the fact that the rate limiting step is associated with cleavage of the first N-O bond of nitrate. We anticipate that stoichiometric investigations of N-O bond cleavage in well-defined molecular complexes will provide insight into this question by delineating mechanistic pathways, in particular insight into product selectivity. In this regard, investigations into the stoichiometric reduction of nitrate ligands have revealed a diversity of products, as determined by both the nature of the metal complex and reducing agent.[7-16]

Reagents for the deoxygenation of ligands by oxygen atom abstraction are especially rare. However, homogeneous reagents based on either silicon ("reductive silylation") or boron ("reductive borylation") can deoxygenate both metal oxides and nitroarenes, and have also been used for reduction and even deoxygenation of metal oxide surfaces.[17-21] An example of this class of reagent is $(BPin)_2pz$, a boron derivative of Mashima's reagent first introduced by Suginome (**Figure 1**), for which the calculated bond dissociation free energies (BDFEs) of the first and second B–N bonds are 87.4 kcal/mol and 61.7 kcal/mol, respectively. It was reported previously that these reagents are capable of reduction without generating salts.[22-25] These relatively weak and polar bonds are easily cleaved in favor of stronger bonds, notably B–O bonds (e.g., BDE = 212 kcal/mol in pinacolborane).[26] Additional thermodynamic driving force for substrate deoxygenation is provided by the energy gain for pyrazine rearomatization. The volatility and solubility of the $O(Bpin)_2$ and pyrazine products also have practical benefits for synthetic chemistry by facilitating product separation.

Together with reductive silylation using Mashima's reagent, we have used the Mashima-Suginome reagent $(BPin)_2pz$ for the reductive borylation of selected transition metal complexes containing coordinated nitrogen oxyanions.[7, 9, 10] It is notable that NO_x^- ligand deoxygenation with these reagents generally stops at the nitrosyl/NO oxidation level. For example, reaction of $(DIM)Fe(MeCN)(NO_3)_2$ (DIM = *N*,*N*′-bis(2,4,6-trimethylphenyl)-1,4-diaza-2,3-dimethyl-1,3-butadiene) with $(BPin)_2pz$ provides the dinitrosyl iron complex (DNIC) $(DIM)Fe(NO)_2$ as the terminal product of the reaction.

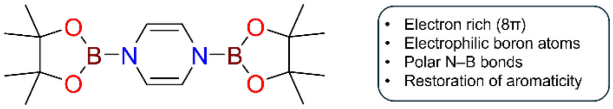

Figure 1. Attractive attributes of the Mashima-Suginome reagent**,** which is a reduced bis(boryl) *N*-heterocycle $(BPin)_2pz$ compound.

In light of these results, we hypothesized that a transition metal system known to stabilize lower oxidation states of nitrogen would enable nitrate reduction beyond the NO oxidation level. For this reason, we decided to investigate nitrate reduction with an iron tris(carbene)borate fragment. This metal fragment is known to support terminal nitrides, leading us to anticipate the conversion of nitrate ligand to nitride.[27] The diverse nitrogen atom transfer reactivity of tris(carbene)borate iron nitride complexes is promising for the synthesis of new organic compounds using the nitrogen atom of nitrate. Beyond the details of this specific system, iron offers multiple metal oxidation states which may help stabilize deoxygenation intermediates, including unanticipated high or low metal oxidation states, thus augmenting the reducing power of the borylation reagent.

We report here the synthesis of the tris(carbene)borate iron(II) nitrate complex $PhB(^iPr_2Im)_3FeNO_3$, where the low steric profile of tris(carbene)borate is expected to allow bulky $(BPin)_2pz$ to access the nitrate ligand. Synthetic investigations reveal that the bis(boryl)pyrazine reagent smoothly deoxygenates the nitrate ligand, sometimes with complementary redox changes at the metal. Interestingly, at least two products are formed, one of which has oxygen shared by iron and boron. This reaction pathway differs from all other reports of nitrate deoxygenation by $(BPin)_2pz$.

RESULTS AND DISCUSSION

Nitrate Ligand Installation

Attempts to prepare a nitrate complex by simple salt metathesis between the known tris(carbene)borate iron chloride complex and various nitrate salts were unsuccessful, with no reaction observed. We therefore devised a different synthetic route in which we anticipated that the reaction of a basic iron complex with an acidic nitrate compound would enable nitrate coordination to iron.

To this end, we prepared and structurally characterized the amido complex $PhB(^iPr_2Im)_3FeNH(^tBu)$ (**1**) as the basic iron source (**Figure 2a, b**). In addition, we devised a new synthesis of anhydrous lutidinium nitrate. Gratifyingly, these compounds reacted cleanly to afford the purple nitrate complex $PhB(^iPr_2Im)_3FeNO_3$ (**2**) in 77 % isolated yield (**Figure 2a**).

The solid-state molecular structure of **2** has been determined by single-crystal X-ray diffraction (**Figure 2c**). Interestingly, despite the potential for being a multidentate ligand, the nitrate ligand in **2** is monodentate. This binding mode is consistent with high spin (S = 2) iron(II) due to the fact that a vacant orbital required for bidentate binding is not available. The nitrate ligand is planar (Σ angles around N = 360°). The Fe-coordinated oxygen is further from nitrogen (N-O 1.316(8) Å) than the other two oxygen atoms of the nitrate ligand (1.257(9) Å and 1.218(8) Å), consistent with localization of N/O π bonds to the terminal oxygens. The Fe-O distance is comparable to that in $PhB(^iPr_2Im)_3FeOSO_2CF_3$ (see SI) while the Fe-C bonds are comparable to those observed in other high spin iron(II) tris(carbene)borate complexes.[28, 29]

Complex **2** has also been spectroscopically characterized. The most notable feature of the high resolution XPS spectrum is the 1s binding energy of the nitrate nitrogen (BE = 406.8 eV), which is comparable to other metal nitrate complexes.[30] The nitrate ligand is further characterized by spectroscopy ($\nu_{N\text{-}O}$ = 1667 cm^{-1} in KBr). The Fe XPS spectrum is consistent with high spin iron(II), with the binding energies for the $2p_{3/2}$ (710.4 eV) and shake-up satellite (713.35 eV) similar to those observed for other iron(II) tris(carbene)borate complexes. The complex has also been characterized by ^1H NMR spectroscopy.[31-33]

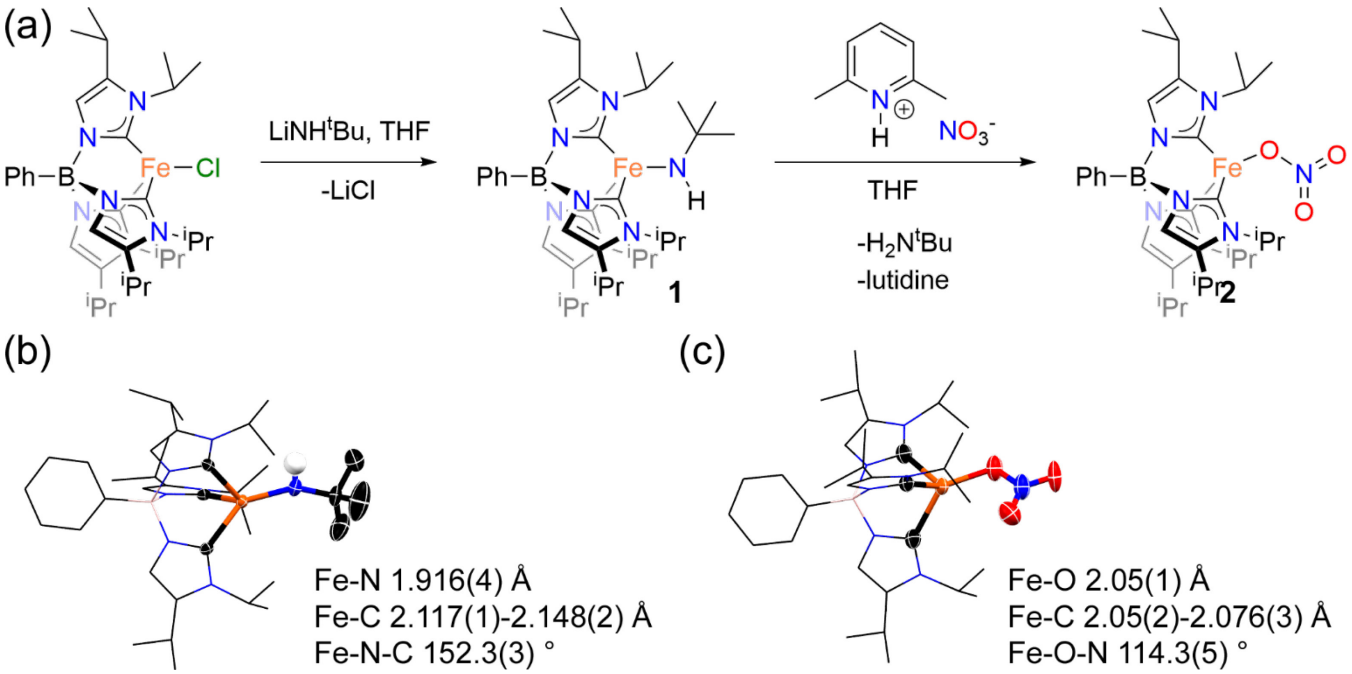

Figure 2. (a) Synthesis of complexes **1** and **2**; single crystal structures of (b) complex **1**; and (c) complex **2**. Thermal ellipsoids shown at 50% probability, most hydrogen atoms omitted, and tris(carbene)borate ligand represented in wireframe for clarity. Color scheme: C, black; N, blue; B, pink; Fe, orange; O, red.

Scheme 1. Deoxygenation of **2** with $(BPin)_2pz$ provides **3** and the proposed complex **4**.

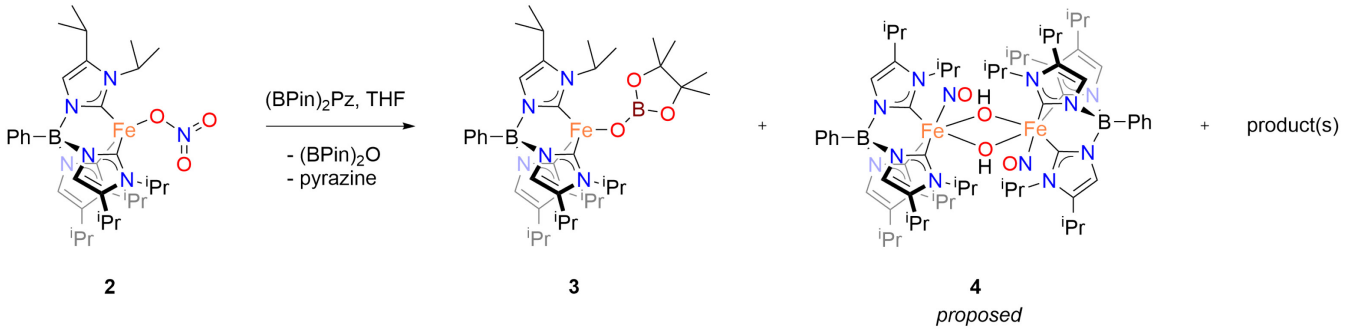

Nitrate Deoxygenation

With complex **2** in hand, we were interested in determining the fate of the nitrate ligand in deoxygenation reactions. Here, we observe that **2** reacts to completion with equimolar $(BPin)_2pz$ within 1 h, providing two major paramagnetic products, **3** and **4**, formed in spectral yields of approximately 70 % and 20 %, respectively (Scheme 1). We were also able to identify pyrazine and the boryl ether $(BPin)_2O$, which are formed in a molar ratio of pyrazine: $(BPin)_2O$ = 10:8. Neither NO nor N_2O were detected in the headspace of the reaction as determined by FT-IR spectroscopy. Importantly, a control experiment reveals that $(BPin)_2pz$ does not react with $NaNO_3$.

Complex **3** has been structurally and spectroscopically characterized. The solid-state molecular structure of **3**, as determined by single-crystal X-ray diffraction, reveals a four-coordinate iron center bound to the tris(carbene)borate ligand and a boralanolate ligand (**Figure 3**), The Fe–O bond distance (1.889(2) Å,) is considerably shorter than that in complex **2**.

The ^{1}H NMR spectrum of **3** is consistent with the solid-state structure. The paramagnetically shifted resonances are consistent with a three-fold symmetric complex and the resonance corresponding to the methyl groups on the OBPin ligand can be assigned by integration. Complex **3** can be independently prepared by the reaction of **1** with equimolar HOBPin in 70 % isolated yield. Importantly, no changes are observed by ^{1}H NMR spectroscopy when complex **3** is treated with excess $Bpin_2pz$. This complex is therefore the terminal reductive borylation product of NO_x deoxygenation.

The formation of complex **3**, which features monoanionic $^{-}$OBPin as a ligand, shows that the oxophilicity of iron becomes competitive with that of boron in the later stages of the NO_x reduction reaction. This also shows that deoxygenation does not necessarily involve the concerted transfer of two boryl groups, as might have been concluded from $O(BPin)_2$, which is a commonly seen reaction product. A product with a single boryl ligand also implicates the intermediacy of mono-boryl pyrazinyl radicals.[34]

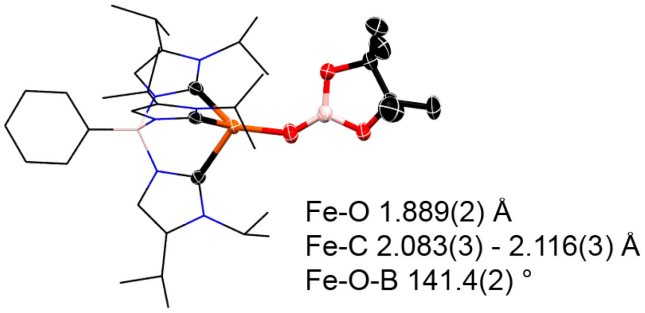

Figure 3. Crystal structure of PhB(^{i}Pr$_2$Im)$_3$FeOBPin (**3**) with thermal ellipsoids at 50% probability. Hydrogen atoms omitted, and tris(carbene)borate ligand is represented in wireframe for clarity. Color scheme: C, black; N, blue; B, light pink; Fe, orange.

We propose complex **4** to be the dinuclear complex [PhB(^{i}Pr$_2$Im)$_3$Fe(NO)(μ-OH)]$_2$ on the basis of spectroscopic and spectrometry data. Multiple attempts to obtain crystals for single crystal X-ray diffraction have been unsuccessful. Characterization of this complex is also complicated by its thermal instability, which decomposes in room temperature solution overnight and a week in the solid state at -35 °C.

The ESI-MS of **4** reveals a mass at m/Z = 1288.7 with an isotopic mass pattern that matches that expected for [PhB(^{i}Pr$_2$Im)$_3$Fe(NO)(μ-OH)]$_2$. This is the formula for the dimer of [PhB(^{i}Pr$_2$Im)$_3$Fe(NO$_2$)] (i.e., the monodeoxygenation product of **2**) plus two hydrogen atoms. The mass spectrum does not depend on whether the compound is synthesized and/or analyzed in THF or THF-d$_8$. In addition, the same mass spectrum is obtained when the reaction of **2** with $(BPin)_2pz$ is conducted in a silylated reaction vessel. This suggests that hydrogen atoms are scavenged from sacrificial tris(carbene)borate ligand in the synthetic reaction.

The X-ray photoelectron spectrum of **4** is consistent with the proposed structure (**Figure 1**). The survey scan provides the Fe:B:N atom ratio (1:1:7), consistent with the empirical formula of **4**. The high-resolution nitrogen 1s region can be deconvoluted into three different nitrogen environments in the ratio 1:3:3. The peak with the highest binding energy (BE = 401.5 eV) is assigned to the nitrosyl nitrogen, where similar binding energies are observed in other complexes.[10] The remaining two peaks (BE = 400.2 eV and 399.6 eV) are assigned to the nitrogen atoms of the NHC donor, as has been observed for other tris(carbene)borate complexes.[32, 35]

The iron 2p spectrum reveals a broad $2p_{3/2}$ signal at 709.7 eV and a $2p_{1/2}$ signal at 723.2 eV, consistent with high spin iron(III). The zero-field ^{57}Fe Mössbauer spectrum of complex **4** provides better insight into the nature of the iron centers. At 80 K, the isomer shift (δ = 0.19 mm/s) and quadrupolar splitting (ΔE_Q = 1.26 mm/s) are indicative of a high spin iron(III) complex (**Figure S18**).

Finally, the solution ^{1}H NMR spectrum reveals that the complex is threefold symmetric in solution, with the number and relative integration of the observed resonances consistent with the proposed structure. Consistent with the mass spectrometry results (above), there is no change in the ^{1}H NMR spectrum when the compound is synthesized and/or analyzed in THF or THF-d$_8$.

A broad band in the solution IR spectrum of **4** provides evidence for a nitrosyl ligand (ν_{NO} = 1680 cm^{-1} in THF)

Experimental and computational mechanistic insight

We propose that the first step of the reaction of **2** with $(BPin)_2pz$ involves oxygen atom transfer from the nitrate ligand to yield the nitrite complex PhB(^{i}Pr$_2$Im)$_3$FeNO$_2$ **5**. This reaction is calculated by density functional theory (B3LYP/def-TZVP) to be thermodynamically favorable (ΔG = -44.6 kcal/mol in THF). At this level of theory, the calculations favor a high spin (S = 2) configuration for **5** with a κ^1-ONO ligand, however the low spin (S = 0) κ^2-O$_2$N isomer is only 2.8 kcal/mol higher in energy. In addition, the κ^1-NO$_2$ (S = 2) and κ^2-ONO (S = 0) linkage isomers are slightly higher in energy at 3.1 kcal/mol and 5.3 kcal/mol, respectively (Table S7).

To experimentally probe the role of **5** in nitrate ligand deoxygenation, we attempted to prepare this complex so that we could investigate its reactivity towards $(Bpin)_2pz$. However, multiple synthetic routes to make this complex all result in the formation of complex **4**, indicating that iron plays a direct role in the deoxygenation of nitrate. For example, attempted ligand metathesis between PhB(^{i}Pr$_2$Im)$_3$FeOTf with equimolar $AgNO_2$ provides complex **4** as the major product of the reaction, as determined by ^{1}H NMR spectroscopy. Other attempted metathesis reactions (e.g., with $PPNNO_2$ and $NaNO_2$) proceed similarly, as does oxidation of the iron(I) synthon [PhB(^{i}Pr$_2$Im)$_3$Fe]$_2$N$_2$ with $AgNO_2$. While we have been unable to structurally characterize **4** by single crystal X-ray diffraction, we have been able to obtain crystals of [PhB(^{i}Pr$_2$Im)$_3$Fe(NO)(^{i}Pr$_2$ImH)]OTf and κ^2-PhB(^{i}Pr$_2$Im)$_2$(^{i}Pr$_2$Im=O)Fe(NO)$_2$ (**Figures S21 and S22**) from these reactions. The formation of these complexes, which involve degradation and/or oxidation of the tris(carbene)borate ligand, is likely a result of the thermal instability of **4,** but they prove the presence of nitrosyl ligands.

Scheme 2. Reaction coordinate for the reaction of **2** with $(BPin)_2pz$ in THF, as computed by DFT (B3LYP/def2-TZVP).

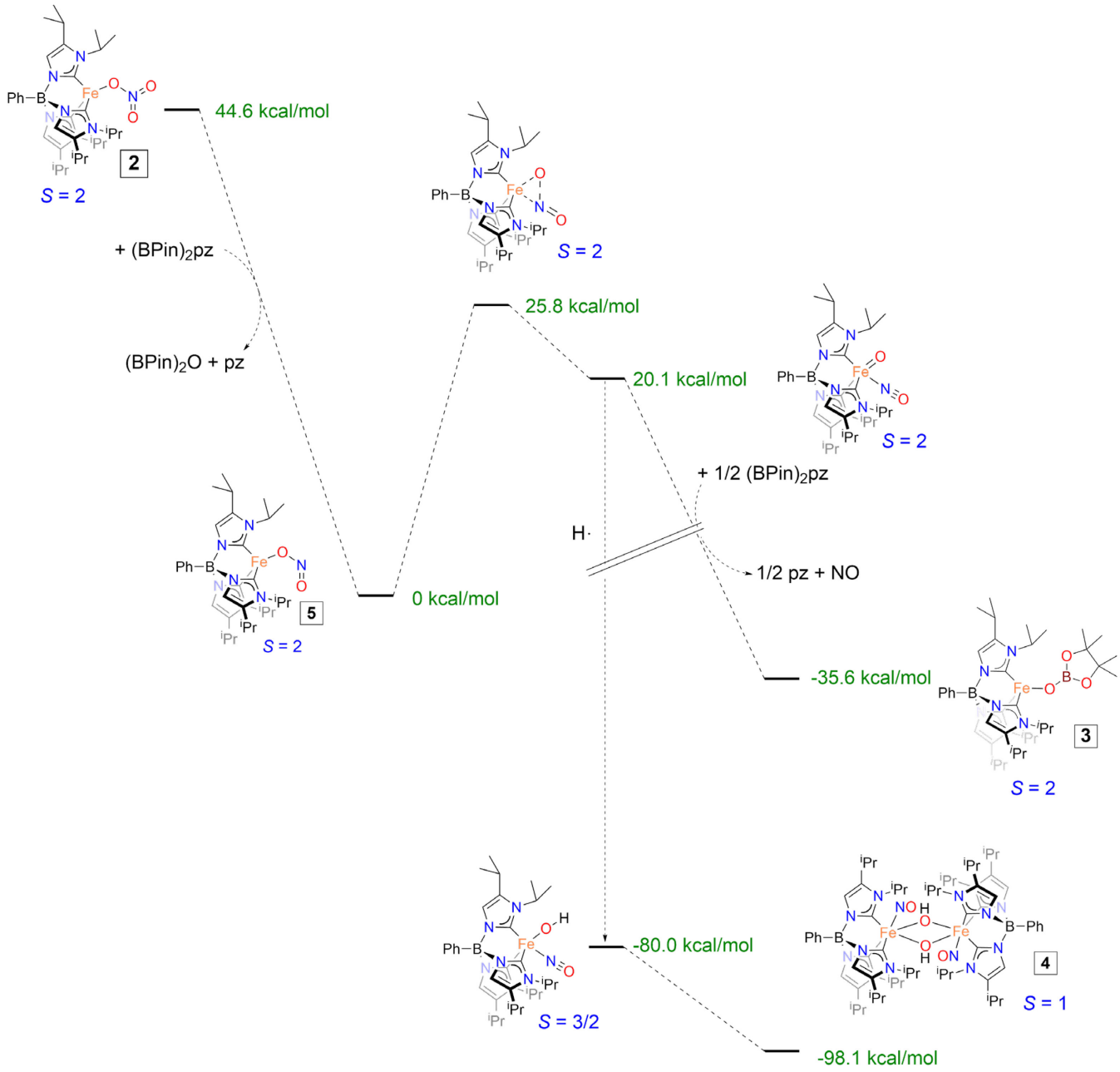

Together, these results suggest that the reaction of **2** with $(BPin)_2pz$ initially provides the nitrite complex **5**, but this species is inherently unstable. In the absence of other reagents **5** decomposes to provide **4**, whereas under the conditions of the nitrate ligand deoxygenation reaction, excess $(BPin)_2pz$ can divert this decomposition to provide complex **3**.

We have computed a pathway for the reaction of **2** with $(BPin)_2pz$ (Scheme 2). Following nitrate ligand deoxygenation to afford **5**, we suggest this complex isomerizes to afford the oxo complex $PhB(^iPr_2Im)_3Fe(NO)(O)$. Here, we were able to locate a transition state on the S = 2 surface. Based on the computed energetics ($\Delta G^{\ddagger}$ = 25.8 kcal/mol, ΔG = 20.1 kcal/mol), this species is likely to be formed in very low concentration. However, there are strong thermodynamic driving forces for the formation of **3** and **4**, as determined by DFT.

We suggest that the formation of **3** involves the reaction of $PhB(^iPr_2Im)_3Fe(NO)(O)$ with $(BPin)_2pz$ along with the loss of NO. Here, we find that the overall reaction is thermodynamically favorable (ΔG = -35.6 kcal/mol). Importantly, a control experiment reveals that complex **3** does not react with NO gas.

To account for the formation of **4**, we suggest that I $PhB(^iPr_2Im)_3Fe(NO)(O)$ is active in hydrogen atom abstraction reactions, similarly to other iron oxo complexes.[36, 37] The formation of **4** can therefore be rationalized by a sequence of reactions involving hydrogen atom transfer to the oxo ligand (e.g., from sacrificial tris(carbene)borate ligand

or from adventitious water) and dimerization. This pathway is also computed to be at thermodynamically favorable, with $\Delta G \leq 98$ kcal/mol (Scheme 2).

Isotopic labeling has been used to elucidate the fate of the nitrate nitrogen atom in the reaction of **2** with $(BPin)_2pz$. Here, the ^{15}N-labeled complex **^{15}N-2** was synthesized from the reaction of $Lut^{15}NO_3$ and **1**. Treating this complex with $(BPin)_2pz$ leads to the appearance of two equally intense resonances in the $^{15}N\{^1H\}$ NMR spectrum of the crude reaction mixture (δ = 372.9 and 371.8 ppm vs $Me^{15}NO_2$). While we are unable to unambiguously assign these resonances, these chemical shifts are consistent with those observed for nitrosyl ligands.[30, 38] Importantly, there is no evidence for the formation of $^{15}N_2$ (δ = -452 ppm vs $Me^{15}NO_2$) within the detection limits of the method. This result rules out reaction pathways in which nitrosyl ligand deoxygenation by $(BPin)_2pz$ provides a nitride ligand that subsequently undergoes N-N coupling to generate N_2. In addition, there is no evidence for the formation of N_2O by ^{15}N NMR (δ = -231/-143 ppm vs $Me^{15}NO_2$)[39] or FT-IR of the reaction headspace. Similarly, there is no evidence for the formation of free NO by FT-IR.

Whereas complex **4** accounts for 40 % the nitrate-derived nitrogen, we recognize the fate of the remainder (that associated with the formation of **3**) is unknown. We suggest that this nitrogen ends up in unidentified nitrate-derived products (see the results of the ^{15}N isotope labeling experiment) and/or products that are below our detection limits.

The proposed mechanism reveals that $PhB(^iPr_2Im)_3Fe(NO)(O)$ represents a bifurcation point in the reaction pathway. Consequently, we expect that the product ratio will be influenced by the relative concentration of $(BPin)_2pz$. Indeed, the mole fraction of complex **3** to complex **4** increases as the ratio of $(BPin)_2pz$ to complex **2** employed is increased (**Table 1)**.

Conclusions

We have successfully synthesized and characterized the target $PhB(^iPr_2Im)_3FeNO_3$ complex, demonstrating that the strategy where a nitrate source with a sacrificial proton is able to install the weak ligand nitrate *via* the liberation of *tert*-butyl amine. The benefit of this strategy includes the formation of volatile organic byproducts which may be easily removed *in vacuo*, rather than the would-be insoluble salt that arises from a salt metathesis reaction.

With the iron nitrate complex, we have shown deoxygenation of nitrate oxygen by reaction with $(BPin)_2pz$. Reaction of iron nitrate with $(BPin)_2pz$ resulted in the formation of two major paramagnetic products, which are identified to be $PhB(^iPr_2Im)_3FeOBPin$ (**3**) and $[PhB(^iPr_2Im)_3Fe(NO)(\mu\text{-}OH)]_2$ (**4**). Both complexes have been well characterized by various spectroscopic techniques such as ^1H NMR, MS, and XPS. The formation of $PhB(^iPr_2Im)_3FeOBPin$ demonstrates the competitive oxophilicity of both iron and boron. Surprisingly however, numerous attempts at generating $PhB(^iPr_2Im)_3FeNO_2$ are met with the formation of complex **4**, illustrating the transient nature of the iron nitrite and highlighting the ease of which this iron nitrite intramolecularly rearranged and abstracts hydrogen atoms to form a bridging di-iron complex bearing nitrosyl and bridging hydroxide ligands. Overall, this remarkable reactivity of iron nitrate showed that this is a viable method for converting the environmentally harmful nitrate anion into a more interesting form of nitrogen.

Collectively, these results show that, in contrast to our published results with nickel, the metal choice of iron here redirects oxygen removal in part from boron to metal. This can be viewed as decreased stoichiometric demand for boron reductant, and any future effort towards catalytic turnover would then demand the development of methods for deoxygenation of iron.

EXPERIMENTAL

General Considerations.

No uncommon hazards are noted. All manipulations were performed under a nitrogen atmosphere by standard Schlenk techniques or in an MBraun Labmaster glove box maintained at or below 1 ppm of O_2 and H_2O. Glassware was dried at 150°C overnight. Acetonitrile, diethyl ether, pentane, tetrahydrofuran, and toluene were purified by the Glass Contour solvent purification system. Before use, an aliquot of each solvent was tested with a drop of sodium benzophenone ketyl in THF solution. Celite was dried overnight at 200°C under vacuum. $PhB(^iPr_2Im)_3FeCl$ was prepared according to literature procedures.[40] All other chemicals were obtained commercially and used as received. Deuterated solvents were purchased from Cambridge Isotope labs. ^1H NMR spectroscopic measurements of air and moisture sensitive compounds were made in J-Young NMR tubes, with the spectroscopic data recorded on Varian 400 MHz NMR spectrometer at 25°C. Spectra of paramagnetic complexes started with 1000 transients stored in block size of 2. Collection was terminated when sufficient signal-to-noise is observed, typically when block size = 50.

For XPS measurement of air sensitive complexes, the sample was loaded on an adhesive surface on a circular plate, which was placed in an air-tight vessel and sealed inside the glovebox before being taken outside and inserted into the instrument. Inside the instrument, the sample is kept at $1x10^{-9}$ torr pressure for measurement. PHI VersaProbe II instrument was used for XPS experiments with a focused monochromatic AlKα source. The X-ray power of 25 W at 15 kV employed for XPS spectra acquisition mode with 100 μm beam size at the take-off angles of 45°and normal X-ray incidence. The instrument work function was tuned to obtain a binding energy (BE) of 83.96.0 eV for Au $4f_{7/2}$ line for metallic gold and the spectrometer dispersion was adjusted to give a BE's of 284.8 eV, 932.62 eV and of 368.2 eV for the C 1s line of adventitious (aliphatic) carbon presented on the non-sputtered samples, Cu $2p_{3/2}$ and Ag $3d_{5/2}$ photoemission lines, respectively. The PHI dual charge neutralization system was used on all samples. The high resolution N1s, B1s, P2p, Fe2p, and C1s spectra were taken with a minimum of 10-60 s scans using 0.1 eV steps and pass energy of 46.95 eV for N1s, 93.9 eV for B1s, N1s, Fe2p, and 23.5 eV for C1s. All XPS spectra were recorded using PHI software SmartSoft –XPS v2.10.2.13 and processed using PHI MultiPack v9.9.0.8 and/or CasaXPS v.2.3.14 using Shirley background. The relative sensitivity factors from MultiPack library were used to determine atomic percentages. Peaks were fitted using GL line shapes, which are a combination of Gaussians and Lorentzians. Wherever possible, conclusions

were drawn from the number of resolved transitions for a given element, to minimize reliance on absolute binding energies for the nonconductive molecular materials. A given sample was examined at 5-6 different spots on the mounted specimen to assure that consistent, reproducible results were obtained.

Mass spectra were recorded using electrospray ionization on a Thermo Electron Corp MAT-95XP spectrometer.

Single crystals for X-ray diffraction were grown by reverse vapor diffusion of diethyl ether from an inner vial containing a solution of the product into a larger vial charged with toluene.

Synthesis of Compounds

Lutidinium nitrate. A 125 mL Erlenmeyer flask was loaded with dry 2,6-lutidine (1.00 g, 9.33 mmol, 1 equiv.) and dry pentane (50 mL). The solution was cooled in an ice water bath. A stir bar was added to the flask, and concentrated HNO_3 (0.65 mL, 10.3 mmol, 1.1 equiv.) was combined dropwise while stirring. The bath was removed and the mixture was allowed to come to room temperature. After 1 h, the pentane was decanted, the white slurry was redissolved in acetonitrile and transferred to a vial. The acetonitrile was removed *in vacuo* to afford pale yellow solids that were purified *via* vacuum sublimation under reduced pressure at 100°C (0.690 g, 43 % yield). ^{1}H NMR (400 MHz, CD_3OD): δ (ppm) 8.35 (t, J_{HH} = 8 Hz,1 H, *p*-C*H*), 7.73 (d, 2 H, J_{HH} = 8 Hz, *m*-C*H*), 2.77 (s, 6 H, *o*-CH_3). FTMS (ESI/Q-TOF) m/z $[Lut]^+[NO_3]^-$ Calcd. for $[Lut]^+$ $C_7H_{10}N$: 108.0808; Found: 108.0808. Calcd. for $[NO_3]^-$: 61.9884. Found: 61.9885. XPS (eV, % area) N 1s: 401.00, 49.87% (lutidinium nitrogen), 406.38, 50.13% (nitrate nitrogen).

PhB(^{i}Pr$_2$Im)$_3$FeNH^{t}Bu (1). Lithium *tert*-butylamide (37 mg, 475 mmol) was added to a yellow solution of PhB(^{i}Pr$_2$Im)$_3$FeCl (200 mg, 316 mmol) in THF (5 mL). The solution stirred overnight with the color of the solution turning deep yellow. The volatiles were removed under vacuum and the resulting yellow solids extracted with pentane and was filtered through Celite. The pentane was removed under vacuum, leaving flaky yellow solid (190 mg, 89 % yield). Crystals suitable for X-ray diffraction were grown by slow diffusion of ether into toluene at -35 °C. ^{1}H NMR (400 MHz, THF-d_8): δ (ppm) 76.0 (s, 9H, N-(CH_3)$_3$, 71.8 (s, 3H, Im-H), 44.6 (s, 2H, B(C_6H_5) o/m-H), 22.2 (s, 2H, B(C_6H_5) o/m-H), 19.2 (s, 1H, B(C_6H_5) p-H), 1.07 (s, 18H, CH(CH_3)$_2$), 0.67 (s, 3H, C*H*(CH_3)$_2$), -3.38 (s, 3H, C*H*(CH_3)$_2$), -34.1 (s, 18H, CH(CH_3)$_2$).

PhB(^{i}Pr$_2$Im)$_3$FeNO$_3$ (2). Lutidinium nitrate (25.4 mg, 0.143 mmol) was added to a yellow solution of PhB(^{i}Pr$_2$Im)$_3$FeNH^{t}Bu (100 mg, 0.143 mmol) in THF (10 mL). The solution was allowed to stir for one hour with the color of the solution changing to deep purple. The volatiles were removed under vacuum, the resulting purple solids washed with pentane and dried (45 mg, 46 % yield). Crystals suitable for X-ray diffraction were grown by slow diffusion of ether into toluene at -35 °C. ^{1}H NMR (400 MHz, THF-d_8): δ (ppm) 46.8 (s, 3H, Im-H), 31.7 (s, 2H, B(C_6H_5) o/m-H), 17.0 (s, 2H, B(C_6H_5) o/m-H), 14.9 (s, 1H, B(C_6H_5) p-H), 1.17 (s, 18H, CH(CH_3)$_2$), 1.02 (s, 3H, C*H*(CH_3)$_2$), -9.41 (s, 3H, C*H*(CH_3)$_2$), -13.8 (s, 18H, CH(CH_3)$_2$). FTMS (ESI/Q-TOF) m/z $[M+H]^+$ Calcd. for $C_{33}H_{51}O_3N_7BFe$: 660.3490; Found: 660.3471.

PhB(^{i}Pr$_2$Im)$_3$FeOBPin (3). 4,4,5,5-Tetramethyl-1,3,2-dioxaborolan-2-ol (21.5 mg, 0.149 mmol) was added to a yellow toluene solution of PhB(^{i}Pr$_2$Im)$_3$FeNH^{t}Bu (100 mg, 0.149 mmol) in toluene (10 mL). The solution was allowed to stir for three hours, during which time the yellow color of the solution faded. The volatiles were removed *in vacuo*, leaving behind a white solid that was washed with pentane and dried under vacuum (60 mg, 55 % yield). Crystals suitable for X-ray diffraction were grown by slow diffusion of ether into toluene at -35 °C. ^{1}H NMR (400 MHz, THF-d_8): δ (ppm) 72.1 (s, 3H, Im-H), 49.3 (s, 2H, B(C_6H_5) o/m-H), 24.5 (s, 12H, B(C_4)(CH_3)$_4$), 24.3 (s, 2H, B(C_6H_5) o/m-H), 20.7 (s, 1H, B(C_6H_5) p-H), -0.51 (s, 18H, CH(CH_3)$_2$), -3.91 (s, 3H, C*H*(CH_3)$_2$), -21.8 (s, 3H, C*H*(CH_3)$_2$), -33.4 (s, 18H, CH(CH_3)$_2$). FTMS (ESI/Q-TOF) m/z $[M+H]^+$ Calcd. for $C_{39}H_{63}O_3N_6B_2Fe$: 741.44917; Found: 741.4495.

Deoxygenation of 2. A solution of **2** (13 mg, 0.020 mmol) in 0.5 mL THF-d_8 was added to a 0.5 mL THF solution of $(BPin)_2pz$ (6.6 mg, 0.020 mmol) in a J-Young NMR tube. The tube was inverted and allowed to mix, resulting in an immediate change in color from purple to brown. The reaction was monitored by ^{1}H NMR spectroscopy. Complete consumption of **2** occurs within 1 h, with concomitant formation of **3** and **4**. The mole ratio between **4** and **3** was found to be 0.35 to 1.

The reaction was repeated with different mole ratios of **2** and $(BPin)_2pz$ ratio. In all cases, **3** and **4** were formed, but in different ratios (Table 1) with the mole ratio between **4** and **3** decreasing from 0.35 to 1 and 0.2 to 1 as the concentration of reducing agent increases. This indicates that as $(BPin)_2pz$ concentration is higher, the formation of product **4** decreases.

Table 1. Effect of reaction stoichiometry (moles) on the product distribution.

Trial	**2**: $(BPin)_2pz$	**3**:**4**
1	1:1	1:0.35
2	1:2	1:0.35
3	1:3	1:0.20

[PhB(^{i}Pr$_2$Im)$_3$Fe(NO)(OH)]$_2$ (4).

Reduction of PhB(^{i}Pr$_2$Im)$_3$FeCl: A yellow solution of PhB(^{i}Pr$_2$Im)$_3$FeCl (200 mg, 316 mmol) in toluene (50 mL) was cooled at -78°C for 30 min. Solid KC_8 (128 mg, 948 mmol) was added to the solution with vigorous stirring. The flask was closed and the reaction stirred for 3 d. The black graphite was removed by filtration to afford a red solution. The solvent was removed *in vacuo* to provide brown solid that was washed with pentane (3 × 10 mL) that we propose to be the iron(I) complex PhB(^{i}Pr$_2$Im)$_3$Fe-N=N-Fe(^{i}Pr$_2$Im)$_3$BPh. No band that can be attributed to ν_{NN} is observed in the IR spectrum.[41] ^{1}H NMR (400 MHz, C_6D_6): δ (ppm) 92.7 (s, 3H, Im-H), 51.4 (s, 2H, B(C_6H_5) o/m-H), 25.7 (s, 2H, B(C_6H_5) o/m-H), 22.0 (s, 1H, B(C_6H_5) p-H), 1.42 (s, 18H, CH(CH_3)$_2$), -0.85 (s, 3H, C*H*(CH_3)$_2$), -1.22 (s, 3H, C*H*(CH_3)$_2$), -9.06 (s, 18H, CH(CH_3)$_2$). We have been unable to obtain X-ray quality crystals of this complex.

Synthesis of [PhB(^{i}Pr$_2$Im)$_3$Fe(NO)(OH)]$_2$: Solid $AgNO_2$ (9 mg, 0.056 mmol) was added to a solution of PhB(^{i}Pr$_2$Im)$_3$Fe-N=N-Fe(^{i}Pr$_2$Im)$_3$BPh (35 mg, 0.028 mmol) in THF (10 mL). The mixture was vigorously stirred for 2 h, with the solution changing in color from dark red to brown along with the formation of a black precipitate. The solution was filtered through Celite and the volatiles removed ***in vacuo***, leaving a brown solid. ^{1}H NMR (400 MHz, C_6D_6): δ (ppm) 45.3 (s, 6H, Im-H), 20.9 (s, 4H, B(C_6H_5) o/m-H), 16.5 (s, 2H, O*H*), 12.5 (s, 4H, B(C_6H_5) o/m-H), 11.4 (s, 2H, B(C_6H_5) p-H), -0.08 (s, 36H, CH(C*H*$_3$)$_2$), -0.5 (s, 6H, C*H*(CH$_3$)$_2$), -1.25 (s, 6H, C*H*(CH$_3$)$_2$), -6.48 (s, 36H, CH(C*H*$_3$)$_2$). FTMS (ESI/Q-TOF) m/z [M]$^+$ Calcd. for $C_{66}H_{102}O_4N_{14}B_2Fe_2$: 1288.70879; Found: 1288.7105.

PhB(^{i}Pr$_2$Im)$_3$FeOTf (6). Thallium triflate (170 mg, 475 mmol) was added to a yellow solution of PhB(^{i}Pr$_2$Im)$_3$FeCl (200 mg, 316 mmol) in THF (10 mL). White precipitate was observed immediately. The solution was stirred overnight, the reaction filtered and dried under vacuum to provide an off-white solid. The solid was washed with pentane and dried under vacuum (200 mg, 85 % yield). Crystals suitable for X-ray diffraction were grown by slow diffusion of ether into toluene at -35°C. ^{1}H NMR (400 MHz, C_6D_6): δ (ppm) 46.9 (s, 3H, Im-H), 33.3 (s, 2H, B(C_6H_5) o/m-H), 18.0 (s, 2H, B(C_6H_5) o/m-H), 15.7 (s, 1H, B(C_6H_5) p-H), 0.94 (s, 18H, CH(C*H*$_3$)$_2$), -0.19 (s, 3H, C*H*(CH$_3$)$_2$), -4.50 (s, 3H, C*H*(CH$_3$)$_2$), -14. (s, 18H, CH(C*H*$_3$)$_2$). ^{19}F NMR (400 MHz, d$_8$-Toluene): δ (ppm) 46.4.

Control Reactions

Reactions with (BPin)$_2$pz

(BPin)$_2$pz and NaNO$_3$: Solid $NaNO_3$ (2 mg, 0.030 mmol) was added to J-Young NMR tube charged with a solution of (BPin)$_2$pz (10 mg, 0.030 mmol) in THF-d$_8$. No color change was observed upon mixing. No reaction is observed after 24 h at 50 °C, as determined by ^{1}H NMR spectroscopy.

(BPin)$_2$pz and NaNO$_2$: Solid $NaNO_2$ (2 mg, 0.030 mmol) was added to a tube charged with a solution of (BPin)$_2$pz (10 mg, 0.030 mmol) in THF-d$_8$. No color change was observed upon mixing. No reaction is observed after 24 h at 50 °C, as determined by ^{1}H NMR spectroscopy.

(BPin)$_2$pz and AgNO$_2$: Solid $AgNO_2$ (5 mg, 0.030 mmol) was added to a J-Young NMR tube charged with a solution of (BPin)$_2$pz (10 mg, 0.030 mmol) in THF-d$_8$. No color change was observed upon mixing, however a black precipitate formed over 3 h, presumed to be metallic silver. The ^{1}H NMR spectrum reveals the complete consumption of (BPin)$_2$pz with concomitant formation of (BPin)$_2$O (d = 1.21 ppm) and pyrazine (d = 8.53 ppm), indicative of deoxygenation. We did not investigate the fate of the remaining nitrogen and oxygen atoms.

(BPin)$_2$pz and AgOTf: A solution of AgOTf (4 mg, 0.0155 mmol) was added in THF-d$_8$ to a J-Young NMR tube. A pale-yellow solution of (BPin)$_2$pz (2.6 mg, 0.008 mmol) in THF-d$_8$ was added, resulting in an immediate color change from pale yellow to dark brown. In addition, a black precipitate that stained the glass was observed, which is presumed to be metallic silver. The ^{1}H NMR spectrum reveals that all the (BPin)$_2$pz had been consumed. Based on the spectral data, we tentatively suggest that the reaction products are equimolar TfOBPin and pz(BPin)OTf , as shown below. ^{1}H NMR (400 MHz, THF-d$_8$): δ (ppm) 1.2 (s, 12H, Pinacol methyl), 1.21(s, 12H, Pinacol methyl), 9.44 (s, 2H, N(C*H*=CH)$_2$N), 9.22 (s, 2H, N(CH=C*H*)$_2$N). ^{19}F NMR (400 MHz, THF-d$_8$): δ (ppm) 136.4, -151.

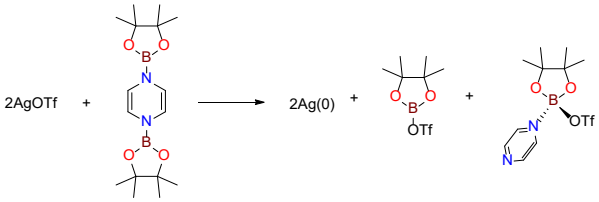

Reactions with NO

Generation and storage of NO. Finely ground Fe(SO$_4$)$_2$•7H$_2$O (1.50 g, 0.01 mmol) was added to a 500 mL Schlenk flask equipped with a Teflon stopper and sidearm adapter connected to a gas manifold. The flask was laid on its side before solid $NaNO_2$ (0.75 g, 0.01 mmol) was carefully layered on the iron sulfate, ensuring that the two reagents do not mix. The Teflon stopper was closed and the flask evacuated under vacuum. The flask was returned to the vertical position to allow the two reagents to mix. Darkening of the solids is observed within minutes. The reaction was left overnight to ensure complete consumption of $NaNO_2$. No red nitrogen dioxide was observed throughout the course of the nitric oxide synthesis, indicating an oxygen free environment. The nitric oxide was stored in the flask and vacuum transferred to reaction vessels as needed.

Reaction with (BPin)$_2$pz. Dissolved gas was removed from J-Young NMR tube containing a solution of (BPin)$_2$pz (8 mg, 0.024 mmol) in THF-d$_8$ via three freeze-pump-thaw rounds. The tube was charged with NO (200 Torr, 0.024 mmol) that was condensed from a calibrated volumetric bulb (1 mL) attached to the gas line. Blue NO was observed to condense on the inside of the NMR tube. The NMR tube was sealed, allowed to warm to room temperature, and inverted to facilitate gas mixing. No color change was observed. No reaction was observed after 2 h at room temperature, as determined by ^{1}H NMR spectroscopy.

Reaction of complex 3. Dissolved gas was removed from J-Young NMR tube containing a solution of **3** (12 mg, 0.016 mmol) in THF-d$_8$ via three freeze-pump-thaw rounds. The solution was charged with 300 Torr (0.016 mmol) of NO gas that was condensed from a calibrated volumetric bulb attached to the gas line. Blue NO was observed to condense inside the NMR tube. The NMR tube was sealed, allowed to warm to room temperature, and inverted to facilitate gas mixing. The reaction was monitored with 1H NMR every hour. No color change was observed. No reaction was observed after 24 h at room temperature, as determined by ^{1}H NMR spectroscopy.

Attempted Detection of N$_2$O .

We attempted to detect the formation of N_2O by gas phase infrared spectroscopy. A 15 cm pathlength transmission cell with ZnSe windows was evacuated to a pressure of 10 mm Hg and 2 mL of the head space of the vial containing the reaction mixture of **2** and (BPin)$_2$pz was injected into the cell. Infrared spectra were collected with a Bruker Optics Vertex 70 Fourier transformed infrared spectrometer. The spectra are reported at 0.5 cm^{-1} resolution and as an average of 128 scans. The limit of detection of detection (3 s) with a 2 mL

injection is 6.0 ppm. The method was first tested and calibrated using authentic samples of nitrous oxide generated from hydroxyl ammonium chloride and sodium nitrite at the same scale as the target reaction. Then, 2 mL of headspace of the reaction between **2** and $(BPin)_2pz$ was injected into the IR cell. No N_2O was observed.

Computational Details.

All calculations were performed using density functional theory as implemented in the ORCA 5.0.1 computational software package.[42, 43] Structures were optimized in the gas phase using the def2-SVP[44] basis set, B3LYP functional, D3BJ dispersion corrections[45, 46] and confirmed to be minima by frequency calculations. Subsequent single point energies were evaluated using the def2-TZVP basis set and the B3LYP functional.

Transition state geometries were determined by the nudged elastic band (NEB) method as implemented in ORCA.[47] Transition states were found to possess only one imaginary frequency and were confirmed by intrinsic reaction coordinate (IRC) calculations.[48]

In the absence of suitable experimental benchmarks, we decided to use the B3LYP functional for our calculations. Previous work from our group has found the B3LYP functional to give reasonable results for related systems,[28, 49, 50] although we appreciate this functional tends to overstabilize high spin states due to the large degree of Hartree-Fock exchange. Since the ground spin state of the structure proposed for complex **4** is not known, all calculations assumed strong ferromagnetic coupling of the two iron centers for an $S = 1$ ground spin state. While the mechanistically-related discussion generally focuses on complexes on the lowest energy high spin (S = 2) surface, lower spin states may be relevant. However, the results for these spin states are qualitatively similar as for the high spin state.

AUTHOR INFORMATION

Corresponding Author

* Kenneth G. Caulton. caulton@iu.edu
* Jeremy M. Smith. smith962@iu.edu

SUPPORTING INFORMATION

Additional tables with crystallographic parameters; ^1H and ^{19}F NMR, XPS, IR, ^{57}Fe Mössbauer, and mass spectra of complexes; computational details and xyz file of computed complexes (PDF).

Accession Codes

CCDC 442581 – 2442586 contains the supplementary crystallographic date for this paper. These data can be obtained free of charge via www.ccdc.cam.ac.uk/data_request/cif or by emailing data_request@ccdc.cam.ac.uk, or by contacting The Cambridge Crystallographic Data Centre, 21 Union Road, Cambridge CB2 1EZ, UK; fax: +44 1223 336033.

ACKNOWLEDGMENT

This work was supported by the National Science Foundation, Chemical Synthesis Program (SYN), by grant CHE-1955887 and the Chemical Catalysis Program (CAT), by grant CHE-2102442. Support for the acquisition of the Bruker Venture D8 diffractometer through the Major Scientific Research Equipment Fund from the President of Indiana University and the Office of the Vice President for Research is gratefully acknowledged. We thank Dr. Arifuzzaman Tapash for his assistance with ^{15}N NMR spectroscopy.

REFERENCES

(1) Galloway, J. N.; Aber, J. D.; Erisman, J. W.; Seitzinger, S. P.; Howarth, R. W.; Cowling, E. B.; Cosby, B. J. The Nitrogen Cascade. *Biosci.* **2003**, *53* (4), 341-356.

(2) Matassa, S.; Batstone, D. J.; Hülsen, T.; Schnoor, J.; Verstraete, W. Can Direct Conversion of Used Nitrogen to New Feed and Protein Help Feed the World? *Environ. Sci. Technol.* **2015**, *49* (9), 5247-5254.

(3) Galloway, J. N.; Leach, A. M.; Bleeker, A.; Erisman, J. W. A chronology of human understanding of the nitrogen cycle. *Philos. Trans. R. Soc. B. Biol. Sci.* **2013**, *368* (1621), 20130120.

(4) Fowler, D.; Coyle, M.; Skiba, U.; Sutton, M. A.; Cape, J. N.; Reis, S.; Sheppard, L. J.; Jenkins, A.; Grizzetti, B.; Galloway, J. N.; et al. The global nitrogen cycle in the twenty-first century. *Philos. Trans. R. Soc. Lond. B. Biol. Sci.* **2013**, *368* (1621), 20130164.

(5) Breitburg, D.; Levin, L. A.; Oschlies, A.; Grégoire, M.; Chavez, F. P.; Conley, D. J.; Garçon, V.; Gilbert, D.; Gutiérrez, D.; Isensee, K.; et al. Declining oxygen in the global ocean and coastal waters. *Science* **2018**, *359* (6371), eaam7240.

(6) Diaz, R. J.; Rosenberg, R. Spreading Dead Zones and Consequences for Marine Ecosystems. *Science* **2008**, *321* (5891), 926-929.

(7) Beagan, D. M.; Carta, V.; Caulton, K. G. A reagent for heteroatom borylation, including iron mediated reductive deoxygenation of nitrate yielding a dinitrosyl complex. *Dalton Trans.* **2020**, *49* (5), 1681-1687.

(8) Moore, J. M.; Miller, T. J.; Mu, M.; Peñas-Defrutos, M. N.; Gullett, K. L.; Elford, L. S.; Quintero, S.; García-Melchor, M.; Fout, A. R. Selective Stepwise Reduction of Nitrate and Nitrite to Dinitrogen or Ammonia. *J. Am. Chem. Soc.* **2025**, *147* (10), 8444-8454.

(9) Cabelof, A. C.; Carta, V.; Caulton, K. G. A proton-responsive ligand becomes a dimetal linker for multisubstrate assembly via nitrate deoxygenation. *Chem. Commun.* **2021**, *57* (22), 2780-2783.

(10) Beagan, D. M.; Cabelof, A. C.; Pepin, R.; Pink, M.; Carta, V.; Caulton, K. G. An Integrated View of Nitrogen Oxyanion Deoxygenation in Solution Chemistry and Electrospray Ion Production. *Inorg. Chem.* **2021**, *60* (22), 17241-17248.

(11) Nakamura, G.; Sakurai, M.; Kametani, Y.; Kawasaki, Y.; Shiota, Y.; Yoshizawa, K.; Ogo, S.; Matsumoto, T. Photosynthesis of NH_3 from NO_3^- Using CH_4 in Homogenous Rhenium Catalysis. *Angew. Chem. Int. Ed. n/a* (n/a), e202423543.

(12) Elrod, L. T.; Kim, E. Lewis Acid Assisted Nitrate Reduction with Biomimetic Molybdenum Oxotransferase Complex. *Inorg. Chem.* **2018**, *57* (5), 2594-2602.

(13) Padmanaban, S.; Chun, J.; Lee, Y.; Cho, K.-B.; Choi, J.; Lee, Y. Nitrate Upcycling Mediated by Organonickel Catalysis. *Angew. Chem. Int. Ed.* **2024**, *63* (39), e202408457.

(14) Mondal, A.; Reddy, K. P.; Som, S.; Chopra, D.; Kundu, S. Nitrate and Nitrite Reductions at Copper(II) Sites: Role of Noncovalent Interactions from Second-Coordination-Sphere. *Inorg. Chem.* **2022**, *61* (50), 20337-20345.

(15) Kulbir; Das, S.; Devi, T.; Goswami, M.; Yenuganti, M.; Bhardwaj, P.; Ghosh, S.; Chandra Sahoo, S.; Kumar, P. Oxygen atom transfer promoted nitrate to nitric oxide transformation: a step-wise reduction of nitrate → nitrite → nitric oxide. *Chem. Sci.* **2021**, *12* (31), 10605-10612.

(16) Gwak, J.; Ahn, S.; Baik, M.-H.; Lee, Y. One metal is enough: a nickel complex reduces nitrate anions to nitrogen gas. *Chem. Sci.* **2019**, *10* (18), 4767-4774.

(17) Kaim, W. Organometal-Stabilized 1,4-Dihydropyrazines: Extremely Electron-Rich Heterocycles. *Angew. Chem. Int. Ed. Eng.* **1981**, *20* (6-7), 600-601.

(18) Kaim, W. Effects of cyclic 8π-electron conjugation in reductively silylated nitrogen heterocycles. *J. Am. Chem. Soc.* **1983**, *105* (4), 707-713.

(19) Saito, T.; Nishiyama, H.; Tanahashi, H.; Kawakita, K.; Tsurugi, H.; Mashima, K. 1,4-Bis(trimethylsilyl)-1,4-diaza-2,5-cyclohexadienes as Strong Salt-Free Reductants for Generating Low-Valent Early Transition Metals with Electron-Donating Ligands. *J. Am. Chem. Soc.* **2014**, *136* (13), 5161-5170.

(20) Hosoya, H.; Misal Castro, L. C.; Sultan, I.; Nakajima, Y.; Ohmura, T.; Sato, K.; Tsurugi, H.; Suginome, M.; Mashima, K. 4,4′-Bipyridyl-Catalyzed Reduction of Nitroarenes by Bis(neopentylglycolato)diboron. *Org. Lett.* **2019**, *21* (24), 9812-9817.

(21) Misal Castro, L. C.; Sultan, I.; Nishi, K.; Tsurugi, H.; Mashima, K. Direct Synthesis of Indoles from Azoarenes and Ketones with Bis(neopentylglycolato)diboron Using 4,4′-Bipyridyl as an Organocatalyst. *J. Org. Chem.* **2021**, *86* (4), 3287-3299.

(22) Tsurugi, H.; Mashima, K. Salt-Free Reduction of Transition Metal Complexes by Bis(trimethylsilyl)cyclohexadiene, -dihydropyrazine, and -4,4′-bipyridinylidene Derivatives. *Acc. Chem. Res.* **2019**, *52* (3), 769-779.

(23) Tsurugi, H.; Mashima, K. A New Protocol to Generate Catalytically Active Species of Group 4–6 Metals by Organosilicon-Based Salt-Free Reductants. *Chem. Eur. J.* **2019**, *25* (4), 913-919.

(24) Bhattacharjee, A.; Hosoya, H.; Yurino, T.; Tsurugi, H.; Mashima, K. Metal-free Reductive Deoxygenation of Sulfoxides by an Organosilicon Reductant, 1,1′-Bis(trimethylsilyl)-1H,1′H-4,4′-bipyridinylidene. *Chem. Lett.* **2019**, *48* (8), 888-890.

(25) Bhattacharjee, A.; Hosoya, H.; Ikeda, H.; Nishi, K.; Tsurugi, H.; Mashima, K. Metal-Free Deoxygenation and Reductive Disilylation of Nitroarenes by Organosilicon Reducing Reagents. *Chem. Eur. J.* **2018**, *24* (44), 11278-11282.

(26) Wang, W.; Lv, Y.; Gou, X.; Leng, X.; Chen, Y. Boron-Oxygen Bond Cleavage of Pinacolborane and Catecholborane Mediated by a Scandium Phosphinidene Complex. *Chin. J. Chem .* **2014**, *32* (8), 752-756.

(27) Scepaniak, J. J.; Fulton, M. D.; Bontchev, R. P.; Duesler, E. N.; Kirk, M. L.; Smith, J. M. Structural and Spectroscopic Characterization of an Electrophilic Iron Nitrido Complex. *J. Am. Chem. Soc.* **2008**, *130* (32), 10515-10517.

(28) Tran, B. G.; Carta, V.; Pink, M.; Caulton, K. G.; Smith, J. M. Facile Addition of B–H and B–B Bonds to an Iron(IV) Nitride Complex. *Inorg. Chem.* **2022**, *61* (49), 19800-19805.

(29) Valdez-Moreira, J. A.; Millikan, S. P.; Gao, X.; Carta, V.; Chen, C.-H.; Smith, J. M. Hydrosilylation of an Iron(IV) Nitride Complex. *Inorg. Chem.* **2020**, *59* (1), 579-583.

(30) Beagan, D. M.; Cabelof, A. C.; Pink, M.; Carta, V.; Gao, X.; Caulton, K. G. Nickel-mediated N–N bond formation and N2O liberation via nitrogen oxyanion reduction. *Chem. Sci.* **2021**, *12* (31), 10664-10672.

(31) Valdez-Moreira, J. A.; Thorarinsdottir, A. E.; DeGayner, J. A.; Lutz, S. A.; Chen, C.-H.; Losovyj, Y.; Pink, M.; Harris, T. D.; Smith, J. M. Strong π-Backbonding Enables Record Magnetic Exchange Coupling Through Cyanide. *J. Am. Chem. Soc.* **2019**, *141* (43), 17092-17097.

(32) Wannipurage, D. C.; Chivington, A. D.; Losovyj, Y.; Pink, M.; Smith, J. M. Synthesis and Reactivity of a Paramagnetic Iron Phosphaethynolate Complex. *Organometallics* **2025**, *44* (3), 468-471.

(33) Ding, M.; Rouzières, M.; Losovyj, Y.; Pink, M.; Clérac, R.; Smith, J. M. Partial Nitrogen Atom Transfer: A New Synthetic Tool to Design Single-Molecule Magnets. *Inorg. Chem.* **2015**, *54* (18), 9075-9080.

(34) Zhang, L.; Jiao, L. Pyridine-Catalyzed Radical Borylation of Aryl Halides. *J. Am. Chem. Soc.* **2017**, *139* (2), 607-610.

(35) Ding, M.; Cutsail III, G. E.; Aravena, D.; Amoza, M.; Rouzières, M.; Dechambenoit, P.; Losovyj, Y.; Pink, M.; Ruiz, E.; Clérac, R.; Smith, J.M. A low spin manganese(iv) nitride single molecule magnet. *Chem. Sci.* **2016**, *7* (9), 6132-6140.

(36) Valdez-Moreira, J. A.; Beagan, D. M.; Yang, H.; Telser, J.; Hoffman, B. M.; Pink, M.; Carta, V.; Smith, J. M. Hydrocarbon Oxidation by an Exposed, Multiply Bonded Iron(III) Oxo Complex. *ACS Cent. Sci.* **2021**, *7* (10), 1751-1755.

(37) Mayer, J. M. Hydrogen Atom Abstraction by Metal–Oxo Complexes: Understanding the Analogy with Organic Radical Reactions. *Acc. Chem. Res.* **1998**, *31* (8), 441-450.

(38) Bell, L. K.; Mason, J.; Mingos, D. M. P.; Tew, D. G. Nitrogen-15 NMR studies of nitrosyl (bent and linear), nitro, and nitrito ligands in 4-, 5-, and 6-coordinate complexes of the platinum metals. *Inorg. Chem.* **1983**, *22* (24), 3497-3502.

(39) Puerta Lombardi, B. M.; Gendy, C.; Gelfand, B. S.; Bernard, G. M.; Wasylishen, R. E.; Tuononen, H. M.; Roesler, R. Side-on Coordination in Isostructural Nitrous Oxide and Carbon Dioxide Complexes of Nickel. *Angew. Chem. Int. Ed.* **2021**, *60* (13), 7077-7081.

(40) Martinez, J. L.; Lin, H.-J.; Lee, W.-T.; Pink, M.; Chen, C.-H.; Gao, X.; Dickie, D. A.; Smith, J. M. Cyanide Ligand Assembly by Carbon Atom Transfer to an Iron Nitride. *J. Am. Chem. Soc.* **2017**, *139* (40), 14037-14040.

(41) Fan Yiming, C. J., Gao Yafei, Shi Min, Deng Liang. Iron Dinitrogen Complexes Supported by Tris(NHC)borate Ligand: Synthesis, Characterization, and Reactivity Study. *Acta Chim. Sin.* **2018**, *76* (6), 445-452.

(42) Neese, F. Software update: The ORCA program system—Version 5.0. *WIREs Comput. Mol. Sci.* **2022**, *12* (5), e1606.

(43) Neese, F. The SHARK integral generation and digestion system. *J. Comput. Chem.* **2023**, *44* (3), 381-396.

(44) Weigend, F.; Ahlrichs, R. Balanced basis sets of split valence, triple zeta valence and quadruple zeta valence quality for H to Rn: Design and assessment of accuracy. *Physical Chemistry Chemical Physics* **2005**, *7* (18), 3297-3305.

(45) Grimme, S.; Ehrlich, S.; Goerigk, L. Effect of the damping function in dispersion corrected density functional theory. *J. Comput. Chem.* **2011**, *32* (7), 1456-1465.

(46) Grimme, S.; Antony, J.; Ehrlich, S.; Krieg, H. A consistent and accurate ab initio parametrization of density functional dispersion correction (DFT-D) for the 94 elements H-Pu. *J. Chem. Phys.* **2010**, *132* (15).

(47) Ásgeirsson, V.; Birgisson, B. O.; Bjornsson, R.; Becker, U.; Neese, F.; Riplinger, C.; Jónsson, H. Nudged Elastic Band Method for Molecular Reactions Using Energy-Weighted Springs Combined with Eigenvector Following. *J. Chem. Theory Comput.* **2021**, *17* (8), 4929-4945.

(48) Ishida, K.; Morokuma, K.; Komornicki, A. The intrinsic reaction coordinate. An ab initio calculation for HNC→HCN and $H^- + CH_4 \rightarrow CH_4 + H^-$ *J. Chem. Phys.* **1977**, *66* (5), 2153-2156.

(49) Hickey, A. K.; Muñoz, S. B.; Lutz, S. A.; Pink, M.; Chen, C.-H.; Smith, J. M. Arrested α-hydride migration activates a phosphido ligand for C–H insertion. *Chem. Commun.* **2017**, *53* (2), 412-415.

(50) Cao, Y.; Valdez-Moreira, J. A.; Hay, S.; Smith, J. M.; de Visser, S. P. Reactivity Differences of Trigonal Pyramidal Nonheme Iron(IV)-Oxo and Iron(III)-Oxo Complexes: Experiment and Theory. *Chem. Eur. J.* **2023**, *29* (42), e202300271.

For Table of Contents Only

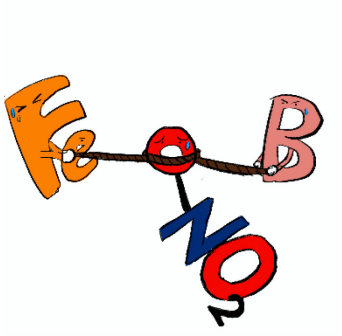

Synopsis: The oxophilicity of iron alters the course of nitrate reduction when $PhB(^{i}Pr_2Im)_3FeNO_3$ is treated with a reducing borane reagent.